HYDROGEN SENSING PROPERTIES OF UV ENHANCED PD-SNO2 NANO-SPHERICAL COMPOSITES AT LOW TEMPERATURE

Peiyu Duan, Zhaoyu Wang, Huahua Xiao*, Jinhua Sun*

State Key Laboratory of Fire Science, University of Science and Technology of China, Hefei, 230026, China, xiaoh@ustc.edu.cn

ABSTRACT

Metal oxide semiconductor (MOS) is promising in developing hydrogen detectors. However, typical MOS materials usually work between 200-500 ℃, which not only restricts their application in flammable and explosive gases detection but also weakens sensor stability and causes high power consumption. This paper studies the sensing properties of UV enhanced Pd-SnO_2 nano-spherical composites at 80-360 ℃. In the experiment, Pd of different molar ratios (0.5, 2.5, 5.0, 10.0) was doped into uniform spherical SnO_2 nanoparticles by a hydrothermal synthesis method. A xenon lamp with a filter was used as the ultraviolet excitation light source to examine the response of the spherical Pd-SnO_2 nanocomposite to 50-1000 ppm H_2 gas. The influence of different intensities of ultraviolet light on the gas-sensing properties of composite materials compared with dark condition was analyzed. The experiments show that the conductivity of the composites can be greatly stabilized and the thermal excitation temperature can be reduced to 180 ℃ under the effect of UV enhancement. A rapid response (4.4/ 17.4 s) to 200 ppm of H_2 at 330 ℃ can be achieved by the Pd-SnO_2 nanocomposites with UV assistance. The mechanism may be attributed to light motivated electron-hole pairs due to built-in electric fields under UV light illumination, which can be captured by target gases and lead to UV controlled gas sensing performance. Catalytic active sites of hydrogen are provided on the surface of the mixed material by Pd. The results in this study can be helpful in reducing the response temperature of MOS materials and improving the performance of hydrogen detectors.

Keywords: Detector; Spherical Pd-SnO_2 nanocomposite；UV enhenced；Hydrogen；Gas sensing properties

1.0 INTRODUCTION

H_2 is known as an important clean energy source which is widely used in many applications such as chemical industries, oil refining, aerospace, and fuel cells [1]. Also, H_2 is one of the main gases evolving under pyrolysis in the initial stage of combustion [2]. Due to the properties of high flammability (0.017 mJ of the ignition energy) and explosiveness, the detection of the hydrogen gas from the leakage is indispensable for safety [3, 4]. In the meantime, as hydrogen energy is beginning to play a greater role in the transition to clean, safe and sustainable energy system, the economic and fast detection of hydrogen in domestic setting is increasingly necessary. A great deal of research has been carried out for hydrogen gas detection such as electrochemical sensors, thermal conductivity sensors, optical sensors, and chemical resistance sensors, etc. [5-7].

Metal–oxide semiconductor nanomaterials such as SnO_2 [8-10], ZnO [11-13], Fe_2O_3 [14, 15], and WO_3 [16, 17], as the typical chemical resistance sensor materials have been widely used for detecting flammable or toxic gases due to their low cost, high sensitivity, and excellent stability. With the advantages of wide bandgap (3.6 eV, which can only respond to UV illumination), simple manufacture and high sensitivity, SnO_2 is considered as a promising candidate for high sensitivity gas detection among all these MOS nanomaterials. Nevertheless, bulk SnO2-based gas sensors have relatively low selectivity, long response/recovery time and poor sensitivity, which hinders its further practical application [18]. To overcome these drawbacks, SnO_2 nanomaterials with tailored microstructure, size and morphology and its composites have been found to be beneficial to the gas sensing performances. Nano-porous materials have well defined porous structure which has been proven to be high gas responsivity and rapid gas responding kinetics in gas sensing devices [19]. With

tailored microstructure, the contacted area between H_2 and sensing materials will be greatly enhanced compared with that using traditional structure. Moreover, the selectivity and response will be improved significantly with the doping of the noble in MOS materials, which have been testified [20-22]. Palladium (Pd) is a suitable catalyst for SnO_2 based sensors for reducing gases typically, which can balance the decreased response to the target gases if water is presented in the surrounding atmosphere [23]. Yang et al. [24] found that the Pd-loaded SnO_2 sensors have magnitude higher resistivity and exhibit significantly enhanced sensitivity to H_2 and lower sensitivity to NO_2 compared to their unloaded counterparts which are attributed to enhanced electron depletion at the surface of the PdO-decorated SnO_2 crystallites and catalytic effect of PdO. Meanwhile, Pd or PdO clusters are usually present at the surface to control the position of the Fermi level for SnO_2.

Furthermore, UV light activation is an effective strategy to realize sensitive properties for room-temperature MOS based gas sensors. In recent years there have been a few reports [25-27] of sensors based on the photo-activation of metal oxide semiconductors. Prades et al. [28] verified that UV light could activate and modulate gas sensing ability of SnO2 nanowires at room temperature, whose sensitivity was comparable with that of the thermally driven device. Wang et al. [27] demonstrated that photo-excitation can increase the carrier density in the conduction band and supply much more active absorption sites on semiconductor surface. In addition, light activation is also very useful to optimize the sensor selectivity and response–recovery speed. Saura [29] described the gas selectivity could be achieved by using filters that modify the UV excitation spectrum. In this regard, light activation is a promising method as an alternative to thermal heating [30]. Few works have been reported to explore the photo-excited H_2 gas sensing properties by combining tailored nanostructures and noble metal with SnO_2.

Herein, Pd was used as a noble metal catalyst doped into the uniform spherical SnO_2 materials. Pure hollow spherical SnO_2 materials and spherical SnO_2 materials with different molar ratios of Pd were synthesized by a facile, template-free, and one-pot hydrothermal method. Different intensities of ultraviolet light were irradiated on the detectors through a xenon light source and a filter of a specific wavelength (365 nm). The H_2 sensing properties of the materials under UV irradiation were systematically examined. Results showed that the response to H_2 can be greatly improved with Pd doping. The response/recovery time was also reduced to 2.2/22.4 s compared to 42.4/42.8 s of the pure spherical SnO_2. The response and recovery time to H_2 could be improved with UV irradiation. Also, the UV irradiation could decrease the response of some typical interfering gases. The optimal intensity of UV irradiation and the H_2 sensing mechanism of UV enhanced uniform spherical Pd-SnO_2 was investigated. This work not only can provide a facile route to synthesize porous spherical Pd-SnO_2 to enhance the property of H_2 sensing, but also may pave a new way for the future design of H_2 detectors with UV irradiation.

2.0 EXPERIMENTAL

2.1 Synthesis and sensor preparation

All the chemical reagents used for preparation of uniform spherical Pd-SnO_2 composites were analytical grade and purchased from Sinopharm Chemical Reagent Co., Ltd, China. The nanocomposites with nominal Pd/Sn atomic ratios in the range of 0-10% were prepared via a facile one-pot hydrothermal synthesis route. In a typical process, 5 mmol (1.7530 g) of $SnCl_4$ $5H_2O$ was dissolved vigorous magnetic stirring into a 9:1 solution of ethanol and deionized water. Appropriate amounts of palladium (II) chloride ($PdCl_2$) were sequentially added by the addition of 0.7 mL of concentrated hydrochloric acid (mass fraction 36.5%) under stirring. The homogeneous mixture solution was obtained after 30 min of ultrasonication, which was after transferred into a 50 mL Teflon-lined stainless steel autoclave and kept at a constant temperature of 200 ℃ for 24 h. The obtained precipitates were washed alternatively with deionized water and ethanol several times by centrifugation to remove the impurity ions, and it were finally dried in vacuum at 60 ℃ for 12 h and calcined at 400 ℃ for 4 h to obtain pristine or Pd-doped SnO2 spherical powders. The obtained samples are hereafter denoted as XPd-SnO_2, where X represents the nominal Pd/Sn atomic ratio

(multiplied by 100) used during the synthesis, e.g., PureSnO_2 for un-doped SnO_2, 0.5Pd-SnO_2 for Pd/Sn of 0.5 at.%, 5.0Pd-SnO_2 for Pd/Sn of 5.0 at.%. Note that while preparing precursors with higher than 10% molar ratio of Pd/Zn, $Pd(Cl)_2$ could not be dissolved completely into solution, leading to formation of uneven doping at the micron level after calcination.

2.2 Characterization

Crystal structures of as-prepared samples were characterized by powder X-ray diffraction (XRD, TTR III) using Cu Kα radiation (λ=0. 15406 nm) at a scanning rate of 10° /min. Crystallite size was estimated by using the Debye-Scherrer formula: $D=0.89\lambda/(\beta\cos\theta)$, where β is the full-width at half maximum (FWHM) of the diffraction peak, λ is the X-ray wavelength used, θ is the Bragg angle, and D is the average crystallite size. Morphology and microstructure of the samples were investigated by scanning electron microscopy (SEM, Gemini SEM 500) equipped with an energy-dispersive X-ray spectrometer (EDX), and transmission electron microscopy (TEM, JEM-2100F).

2.3 Sensor preparation and testing

To ensure the uniformity and repeatability of the detectors, 30 mg of the SnO_2-based materials and 1 mL terpineol were mixed well by ultrasonication for 40 minutes. 30 microliters of suspension droplets were drawn on the Au interdigital electrode with a pipette. The as-prepared sheets were put in an oven at 80 ℃ to dry for 6 h. After that, the dried detectors were put into a muffle furnace 350 ℃ for 3 h with a heating rate of 2℃/min, and cooled to room temperature naturally. Before gas-sensing testing, all the obtained sensors were aged at 300 ℃ for 5 days to achieve stable performance.

The resistance of the as-prepared sensors was measured by a JF02F gas sensing test system (Kunming GuiYanJinFeng Tech. Corp., Ltd.) with 8V bias voltage. The bottom of the Au-IDE is a close-fitting heater, which can realize accurate temperature control. The total gas flow rates of all the experiments were kept at 200 mL/min, which was well controlled by the matched MFC. After the analyte gases (H_2, CH_4, SO_2, etc.) tests were completed, the flow was swiftly switched to 200 mL/min air for recovery. Above the gas chamber is a circular window with a diameter of ~40mm made of quartz glass, which makes the UV lights irradiated to the surface of the detectors. Different intensities of ultraviolet radiation were achieved by controlling a xenon light source (PerfectLight, PLS-SXE 300) and 365nm filter with a controller and a shading plate. The gas sensing response was defined as S= Ra/Rg or Rg/Ra (all the tested oxidizing gases), where Ra is the sensor resistance in reference air, and Rg the resistance in presence of target gas. The response (recovery) time (t_{90}) was the time that the resistance variation reached 90% of the total value after introduction (removal) of the analysed gas. The tested gases and synthetic air used were all customized dry gases with a certain concentration. The radiation intensity on the surfaces of the sensors was measured by an ultraviolet ray meter (Beijing Shida Photoelectric Technology Co., Ltd., UV-A).

3.0 RESULTS AND DISCUSSION

3.1 Phase structure and composition

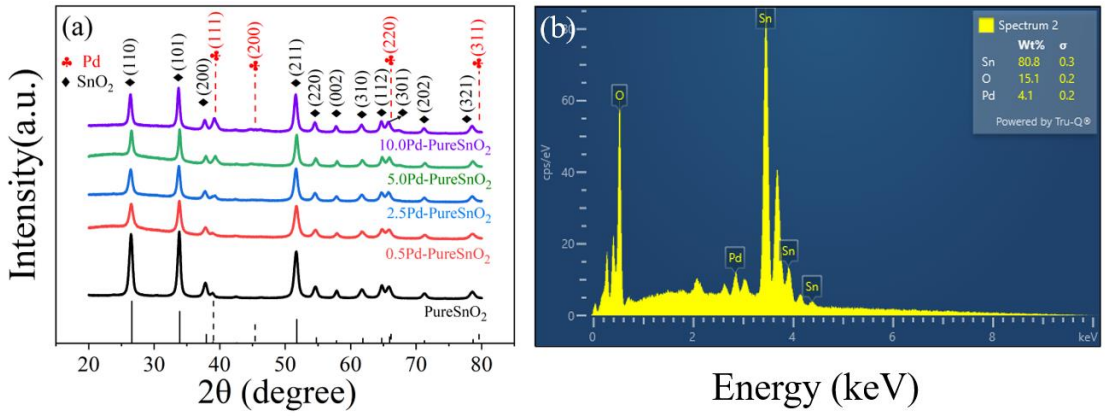

Figure 1. (a) XRD patterns of pure SnO_2 and different molar ratio Pd doped SnO_2, (b) EDX spectrum of 5.0Pd-SnO_2.

To characterize the crystal structures and chemical composition of the as-prepared samples, the XRD patterns and EDX spectra were analyzed and the results were shown in Fig. 1. Fig. 1a shows the XRD spectra obtained from different molar ratio of Pd doped SnO_2, in which the standard cards were shown at the bottom of the picture (solid line for SnO_2 and dashed line for Pd). Correspondingly, All XRD spectra peaks can be well indexed to the crystal surfaces of cassiterite SnO_2 (JCPDS card no. 41-1445) and Pd (JCPDS card no.87-0637) without any extra peak from any impurity. The strength of (111) and (220) surfaces of Pd can be found enhanced significantly with the increase of Pd doping ratio. Noted that the XRD pattern of the 0.5 mol% Pd doped SnO_2 shows almost no change compared with that of the pure SnO_2 which may be due to the small doping ratio. These Pd diffraction peaks are present in the Pd-SnO_2 composite without any shifts, indicating that the Pd dopants are merely placed on the surfaces of the crystals rather than being covalently anchored into the crystal lattices, and further demonstrating the formation of Pd-SnO_2 composite[19]. EDX spectra (Fig. 1b) of the 5.0Pd-SnO_2 composite indicate the presence of Pd, Sn and O in the nanoparticle, which is previously confirmed by the XRD spectra, and the quantitative analysis shows that the molar ratio of Pd and Sn is 5.7%, which matches the theoretical value very well while taking local inhomogeneous mixing into account.

3.2 Microstructure

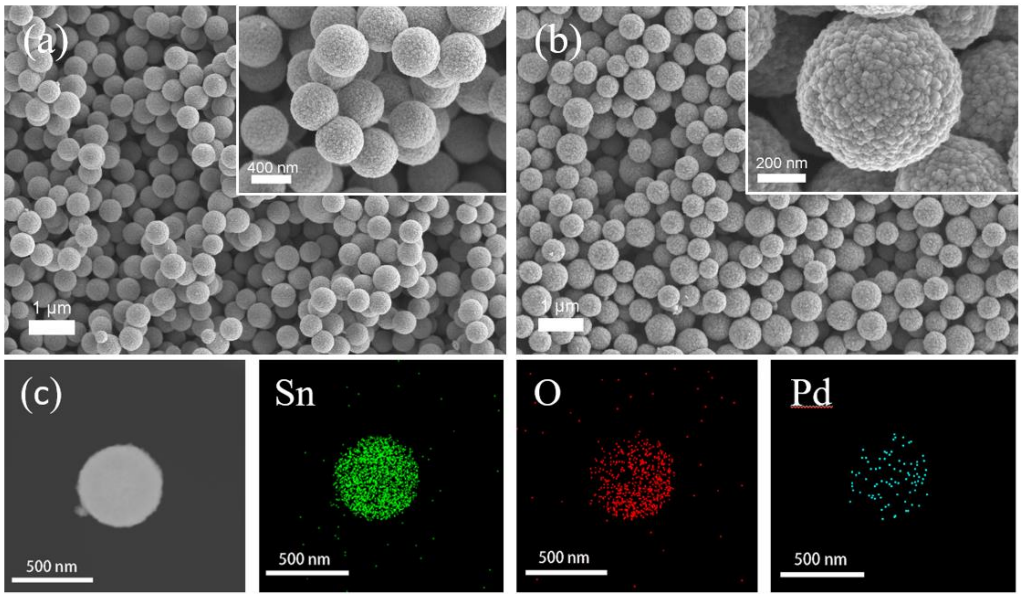

Figure 2. SEM images of (a) hollow spherical SnO_2, (b) spherical 5.0Pd-SnO_2. (c) Elemental mapping of 5.0Pd-SnO_2 sample.

SEM images were employed to investigate the morphology of the pure SnO_2 hollow sphere and 5.0 mol% Pd-SnO_2 porous spherical materials in Fig. 2. The insets showed the magnification images of the local area. Well-separated uniform microspheres with a diameter of about 500 nm were observed in Fig. 2a for the pure SnO_2. Fig. 2b shows that the uniform spherical morphology has not been affected by 5.0 mol% Pd doping. Compared with the pure spherical SnO_2, the particle size of the Pd-doped material is between 500-600 nm, and the surfaces of the materials are rougher, which may provide more activation sites for the reaction. According to elemental mapping of 5.0Pd-SnO_2 sample (Fig. 5c), Sn, O, and Pd elements distributed uniformly throughout the spheres.

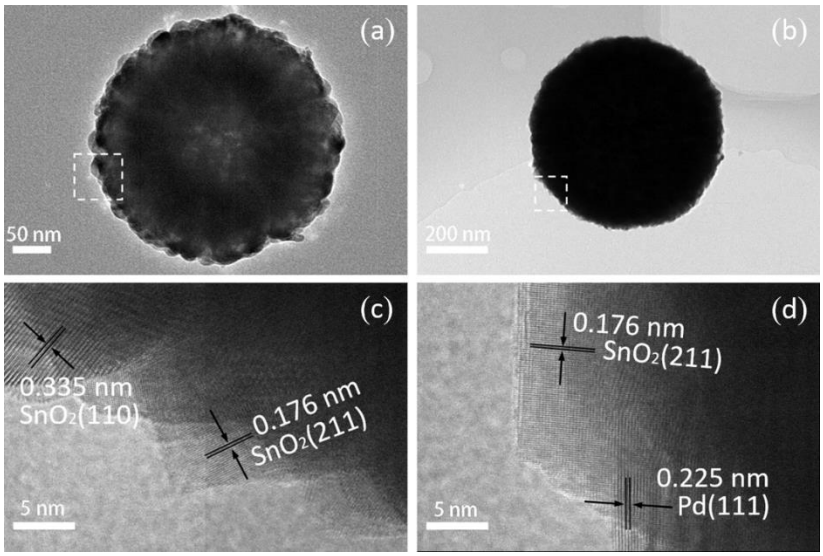

Figure 3. (a, b) TEM and (c, d) HRTEM images of (a, c) hollow spherical SnO_2, (b, d) spherical 5.0Pd-SnO_2.

Typical TEM images of the samples are presented in Fig. 3. The hollow structure of the as-synthesized SnO_2 spheres with a shell thickness about 100 nm was shown in Fig. 3a. It could be seen

in Fig. 3b that the hollow structure of the as-synthesized spheres was altered to solid structure with 5.0 mol% Pd doping. In order to further examine the morphology, structure and lattice fringes, high resolution TEM (HRTEM) of pure SnO_2 and 5.0Pd-SnO_2 were presented in Fig. 3c and Fig. 3d. HRTEM observation presented inter-planar spacing of 0.176 nm and 0.225 nm (Figure 3d), corresponding to the (211) and (111) planes of SnO_2 and Pd, respectively. The presence of Pd and its doping state on the surface of SnO_2 could be observed from Fig. 3d, which was consistent with the results obtained by the XRD and EDS.

3.3 H_2 sensing property

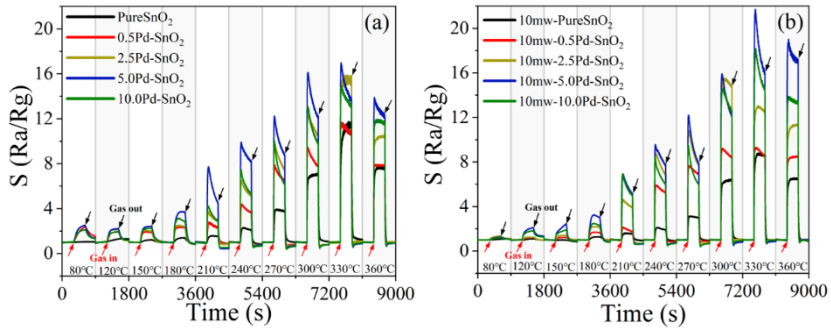

Figure 4. Response of uniform spherical SnO_2 based sensors toward 200 ppm H_2 under different operating temperatures, (a) in dark condition and (b) under 10mW UV irradiation.

Fig. 4a presents the temperature dependence of the gas response to 200 ppm H_2 for the as-prepared sensors in dark condition. Compared with pure SnO_2, sensors' response to hydrogen could be greatly improved with Pd doping. The responses of as-prepared sensors increased with the increase of operating temperatures, and as the response values reached the maximum, the response values decreased with the increase of operating temperatures. Apparently, all the as-prepared sensors achieved the best response at 330 ℃, and the best responses to 200 ppm H_2 were 10.3 and 15.2 for pure SnO_2 and 5.0Pd-SnO_2 in dark condition, respectively. The 5.0 mol% Pd-doped SnO_2 showed the best response to 200 ppm H_2 among all the as-prepared sensors. The responses of Pd-doped sensors had no obvious positive correlation with the increase in temperature below 180 ℃, while the pure SnO_2 had no obvious response. The responses of Pd doped SnO_2 sensors could reach 3~5 for 200 ppm H_2 at 180 ℃ which exceeds the requirements of most commercial MOS detectors. With the illumination of 10 mW/cm^2 UV light in Fig. 4b, the responses of Pd-doped sensors to hydrogen were enhanced at the optimum operating temperature(18.5 for 10mw-5.0Pd-SnO_2 at 330 ℃ compared to 16.5 for 5.0Pd-SnO_2 at 330 ℃), but no obvious enhancement effects were found at lower temperatures. Fig. 4b shows that the UV illumination has no obvious effect on the optimal operating temperature.

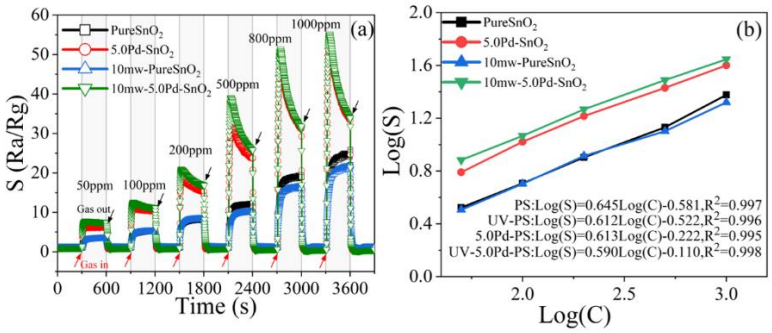

Figure 5. (a) Dynamic response-recovery curves of the as-prepared gas sensors to H_2 in the range of 50 ppm–1000 ppm at 330 ℃, (b) corresponding log(S)~log(C) of different concentrations of H_2.

To check for the linearity of responses with H_2 concentrations, the responses of pure SnO_2 and 5.0Pd-SnO_2 sensors exposed to a wide range of H_2 concentrations from 50 ppm to 1000 ppm in different condition at 330 ℃ were shown in Fig. 5. The dynamic response-recovery curves of the as-prepared gas sensors were shown in Fig. 5a. All the responses of sensors increased with the increasing concentration. The responses of 5.0 mol% Pd-doped sensor showed a significant enhancement compared to the pure SnO2 in both dark and 10 mW UV illumination. The responses to 50 ppm H_2 were 3.21 and 7.63 for pure SnO_2 and 5.0Pd-SnO_2 under 10 mW/cm^2 UV illumination, while the values were 3.34 and 6.18 in dark condition. The UV light shows enhancement effects to the Pd-doped sensors, while the opposite is true for pure SnO_2. Fig. 5b shows the logarithmic curves of the concentration and response values, in which the inset shows the fitting formulas and R-squared values. All the as-prepared sensors under different conditions showed an approximately linearity in the concentration range of 50-1000 ppm. This linear dependence is favorable for calibration and determination of the gas concentration in practical applications [31], which indicates the great potential for quantitative detection of H_2 at ppm level.

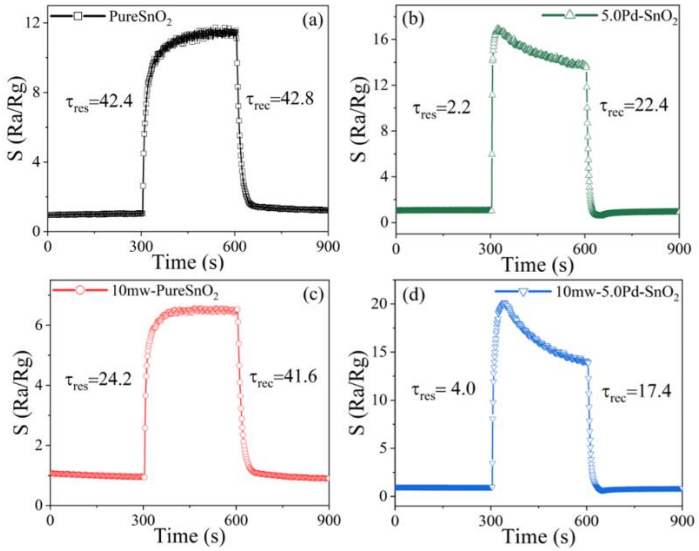

Figure 6. Response transients of gas sensors toward 200 ppm H_2 at 330 ℃, (a) PureSnO_2, (b) 5.0Pd-SnO_2, (c) 10mw-PureSnO_2, (d) 10mw-5.0Pd-SnO_2.

Fig. 6 displays the response transients of gas sensors toward 200 ppm H_2 at 330 ℃, in which both the Pd doping and the UV illumination influences could be observed. Apart from the enhancement of the response values, the response/recovery time is also reduced significantly with the doping of 5.0 mol% Pd, which from 42.4/42.8 s to 2.2/22.4 s (Fig. 6a and Fig. 6b). And for the effects of UV illumination, the response time reduction occurs on pure SnO_2 (Fig. 6a and Fig. 6c), while the recovery time is reduced to 5.0Pd-SnO_2 (Fig. 6b and Fig. 6d). It could be found from Fig. 6 that the doping of 5.0 mol% Pd modified the material, which made a huge change in the sensitivity to hydrogen, while ultraviolet illumination enhanced some of its properties. Reversibility and long-term stability tests of as-prepared gas sensors toward 200 ppm H_2 at 330 ℃ were carried out, as shown in Fig. 7. A measurement of six continuous cycles at 330 ℃ under different conditions could be seen in Fig. 7a, the dynamic response-recovery features were well repeated indicating its good reversibility. Long-term stability is another key factor for practical applications of a gas sensor. As shown in Fig. 7b, the response of the as-prepared sensors to 200 ppm H_2 at 330 ℃ fluctuated slightly in a small range within 60 days. The responses of the sensors fluctuated around 7.95, 10.28, 14.5, and 18.14 for the 10mw-PureSnO_2, PureSnO_2, 5.0Pd-SnO_2, and 10mw-5.0Pd-SnO_2, respectively. The maximum deviations in sensor response can be controlled lower to 5%, indicating the promising long-term stability of the as-prepared sensors for H_2 detecting.

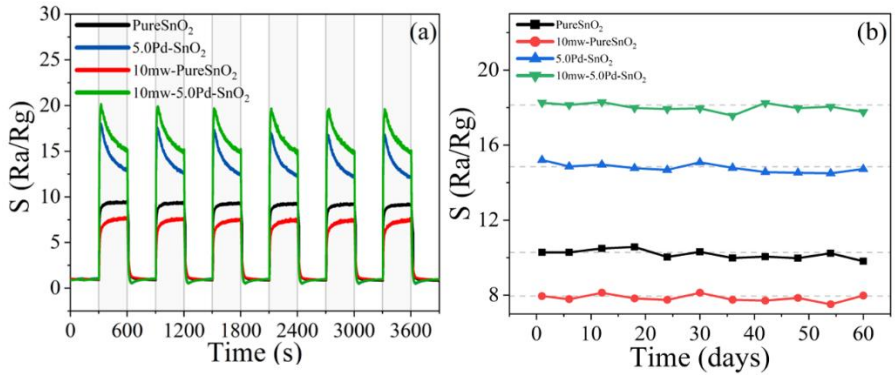

Figure 7. (a) Reversibility of uniform spherical SnO_2 based sensors toward 200 ppm H_2 at 330 ℃, (b) long-term stability tests of as-prepared gas sensors toward 200 ppm H_2 at 330 ℃ nearly 60 days.

Furthermore, the selectivity of as-fabricated gas sensors were tested toward 200 ppm of CH_4, CO, and SO_2, which were the interference gases that are often encountered in homes or car exhausts, as shown in Fig. 8a. It could be found that the 10mw-5.0Pd-SnO_2 showed the best response to 200 ppm H_2 at 330 ℃. The 5.0Pd-SnO_2 showed an enhanced response to 200 ppm H_2 compared to the PureSnO_2, which showed the best response to 200 ppm CH_4. Particularly, the UV illumination could reduce the response of the as-prepared sensors to CH_4 significantly, which provides a new solution to improve the selectivity of the sensors for domestic setting. Outstanding selectivity was achieved by the porous microstructure combined with UV illuminating assistance. The excellent stability of the as-prepared sensors, in combination with its high sensitivity and selectivity, makes it promising for practical application.

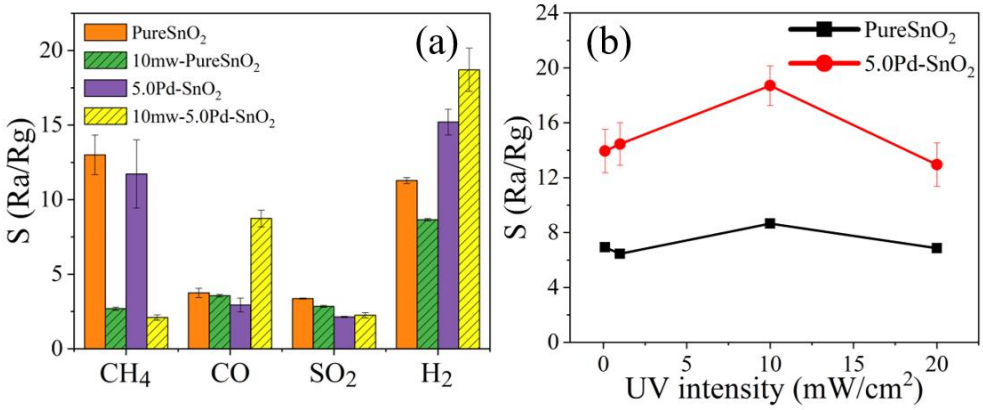

Figure 8. (a) Cross-sensitivities of as-prepared gas sensors to 200 ppm various gases at 330 ℃. (b) Response of pure and 5.0 mol% Pd doped SnO_2 to 200 ppm H_2 under different UV intensities at 330℃.

To study the influence of different UV irradiation intensities on hydrogen detection, the response curves of pure and 5.0 mol% Pd doped SnO_2 to 200 ppm H_2 under 0.1, 1.0, 10.0, and 20.0 mW/cm^2 UV illumination at 330 ℃ were shown in Fig. 8b. The faint UV irradiations were not enough to promote gas adsorption and desorption to enhance the response, while strong UV irradiations would increase the density of photo-generated electron-hole pairs inside the materials, thereby reducing the depletion layer of the material which results in a decrease in gas response. There is an optimum value for UV irradiation, which is 10 mW/cm^2 in this experiment.

The mechanism of as-prepared sensors could be the adsorbed oxygen molecules capture electrons (e-) from the conduction band of gas sensing material due to its strong electronegativity, and transform them into more active chemisorbed oxygen ions (O^-_{2ads}, O^-_{ads}, or O^{2-}_{ads}). It will result in the formation of the space charge region (electron depletion layer), which promotes a substantial increase in the initial

resistance. Upon exposure to a reducing gas, the adsorbed oxygen species, being highly metastable, oxidize the reducing gas (in this case H2) with these chemisorbed oxygen species, releases the bound electrons back to the conduction band as free electrons, and subsequently lowers the resistance of the SnO_2-based sensors [32]. The Pd on the surfaces of crystalline provided more activation sites for the reaction, while the UV illumination promoted the adsorption and desorption of gases, and enhanced some properties of hydrogen sensing. Further discussion of the mechanism will not be described here, which has been explained in some research [33-35].

4.0 CONCLUSION

Uniform hollow spherical SnO_2 and Pd-doped porous microspheres were prepared via a template-free one-pot hydrothermal method. Gas sensing measurements indicated that the Pd-doped sensors were sensitive to the presence of H_2 gas. All data indicated that the response of 5.0 mol% Pd-SnO_2 composite was the highest among the as-prepared samples, the sensor based on 5.0 mol% Pd-SnO_2 exhibits high sensitivity of 18.50 toward 200 ppm H_2 at an operating temperature of 330 ℃, which is about 1.80 times higher than pure SnO_2. The Pd-doped sensors showed good properties even at a low temperature of 180 ℃, which makes it a potential low consumption and safer H_2 detector for domestic setting. In addition, fast response and recovery times (2.2 s/ 22.4 s) were achieved with the 5.0Pd-SnO_2. Particularly, the 10 mW/cm^2 UV illumination not only enhanced the response of Pd-doped sensors at high temperature, but improved its response/recovery time and selectivity to hydrogen, which paved a new way for the future design of H_2 detectors with UV irradiation. Also, there is an optimal UV intensity for the as-prepared sensors, which was related to the principle of metal oxide semiconductor gas sensing. This research not only provided a facile, template-free, and one-pot hydrothermal method to prepare Pd-doped sensitive materials with uniform and special micromorphology, but also explored the effects of UV irradiation for H_2 sensitive properties. This research may provide a potential method for the further preparation of hydrogen sensors with high selectivity, high sensitivity and low power consumption.

ACKNOWLEDGEMENTS

This study was supported by the Fundamental Research Funds for the Central Universities (Grant No. WK2320000048).

REFERENCES

1. H. Xun, Z. Zhang, A. Yu, J. Yi, Remarkably enhanced hydrogen sensing of highly-ordered SnO_2-decorated TiO_2 nanotubes, Sensors and Actuators B: Chemical, 273 (2018) 983-990.
2. S. Krüger, M.-C. Despinasse, T. Raspe, K. Nörthemann, W. Moritz, Early fire detection: Are hydrogen sensors able to detect pyrolysis of house hold materials?, Fire Safety J, 91 (2017) 1059-1067.
3. S.F. Silva, L. Coelho, O. Frazao, J.L. Santos, F.X. Malcata, A Review of Palladium-Based Fiber-Optic Sensors for Molecular Hydrogen Detection, Ieee Sens J, 12 (2012) 93-102.
4. M. Zhang, Y. Zhen, F. Sun, C. Xu, Hydrothermally synthesized SnO2-graphene composites for H_2 sensing at low operating temperature, Materials Science and Engineering: B, 209 (2016) 37-44.
5. M. Tiemann, Porous metal oxides as gas sensors, Chemistry, 13 (2007) 8376-8388.
6. T. Hübert, L. Boon-Brett, V. Palmisano, M.A. Bader, Developments in gas sensor technology for hydrogen safety, International Journal of Hydrogen Energy, 39 (2014) 20474-20483.
7. L. Boon-Brett, J. Bousek, G. Black, P. Moretto, P. Castello, T. Hübert, U. Banach, Identifying performance gaps in hydrogen safety sensor technology for automotive and stationary applications, International Journal of Hydrogen Energy, 35 (2010) 373-384.
8. H. Zhang, Z. Li, J. Yi, H. Zhang, Z. Zhang, Potentiometric hydrogen sensing of ordered SnO_2 thin films, Sensors and Actuators B: Chemical, 321 (2020).

9. C. Liewhiran, N. Tamaekong, A. Tuantranont, A. Wisitsoraat, S. Phanichphant, The effect of Pt nanoparticles loading on H_2 sensing properties of flame-spray-made SnO_2 sensing films, Materials Chemistry and Physics, 147 (2014) 661-672.
10. J.Y. Jie Hu, Wenda Wang, Yan Xue, Yongjiao Sun, Pengwei Li, Kun Lian, Wendong Zhang, Lin Chen, J.S. , Yong Chen, Synthesis and gas sensing properties of NiO/SnO_2 hierarchical structures toward ppb-level acetone detection, Materials Research Bulletin, 102 (2018) 294–303.
11. L. Zhu, W. Zeng, Room-temperature gas sensing of ZnO-based gas sensor: A review, Sensors and Actuators A: Physical, 267 (2017) 242-261.
12. L. Wang, H. Dou, F. Li, J. Deng, Z. Lou, T. Zhang, Controllable and enhanced HCHO sensing performances of different-shelled ZnO hollow microspheres, Sensors and Actuators B: Chemical, 183 (2013) 467-473.
13. P.S. Shewale, K.-S. Yun, Synthesis and characterization of Cu-doped ZnO/RGO nanocomposites for room-temperature H_2S gas sensor, Journal of Alloys and Compounds, 837 (2020).
14. P. Sun, Y. Cai, S. Du, X. Xu, L. You, J. Ma, F. Liu, X. Liang, Y. Sun, G. Lu, Hierarchical α-Fe_2O_3/SnO_2 semiconductor composites: Hydrothermal synthesis and gas sensing properties, Sensors and Actuators B: Chemical, 182 (2013) 336-343.
15. S.T. Navale, D.K. Bandgar, S.R. Nalage, G.D. Khuspe, M.A. Chougule, Y.D. Kolekar, S. Sen, V.B. Patil, Synthesis of Fe_2O_3 nanoparticles for nitrogen dioxide gas sensing applications, Ceramics International, 39 (2013) 6453-6460.
16. S. Haviar, Š. Chlupová, P. Kúš, M. Gillet, V. Matolín, I. Matolínová, Micro-contacted self-assembled tungsten oxide nanorods for hydrogen gas sensing, International Journal of Hydrogen Energy, 42 (2017) 1344-1352.
17. M. Wang, Y. Wang, X. Li, C. Ge, S. Hussain, G. Liu, G. Qiao, WO_3 porous nanosheet arrays with enhanced low temperature NO_2 gas sensing performance, Sensors and Actuators B: Chemical, 316 (2020).
18. S. Singkammo, A. Wisitsoraat, C. Sriprachuabwong, A. Tuantranont, S. Phanichphant, C. Liewhiran, Electrolytically exfoliated graphene-loaded flame-made Ni-doped SnO_2 composite film for acetone sensing, ACS Appl Mater Interfaces, 7 (2015) 3077-3092.
19. L. Yao, Y. Li, Y. Ran, Y. Yang, R. Zhao, L. Su, Y. Kong, D. Ma, Y. Chen, Y. Wang, Construction of novel Pd–SnO_2 composite nanoporous structure as a high-response sensor for methane gas, Journal of Alloys and Compounds, 826 (2020).
20. Liping Yang, Xinyuan Zhou, Xiaofeng Wu, Ning Han and Yunfa Chen, Synthesis of Pd-loaded mesoporous SnO_2 hollow spheres for highly sensitive and stable methane gas sensors, RSC Advances, 8 (2018) 24268–24275.
21. S. Nasresfahani, M.H. Sheikhi, M. Tohidi, A. Zarifkar, Methane gas sensing properties of Pd-doped SnO_2/reduced graphene oxide synthesized by a facile hydrothermal route, Materials Research Bulletin, 89 (2017) 161-169.
22. R. Peng, J. Chen, X. Nie, D. Li, P. Si, J. Feng, L. Zhang, L. Ci, Reduced graphene oxide decorated Pt activated SnO_2 nanoparticles for enhancing methanol sensing performance, Journal of Alloys and Compounds, 762 (2018) 8-15.
23. J.P. Cheng, J. Wang, Q.Q. Li, H.G. Liu, Y. Li, A review of recent developments in tin dioxide composites for gas sensing application, Journal of Industrial and Engineering Chemistry, 44 (2016) 1-22.
24. I.K. Dae-Jin Yang , Doo Young Youn , Avner Rothschild , and Il-Doo Kim, Ultrasensitive and Highly Selective Gas Sensors Based on Electrospun SnO_2 Nanofibers Modified by Pd Loading, Adv. Funct. Mater., 20 (2010) 4258-4264.
25. B. Liu, Y. Luo, K. Li, H. Wang, L. Gao, G. Duan, Room-Temperature NO_2 Gas Sensing with Ultra-Sensitivity Activated by Ultraviolet Light Based on SnO_2 Monolayer Array Film, Advanced Materials Interfaces, 6 (2019).

26. L. Liu, X. Li, P.K. Dutta, J. Wang, Room temperature impedance spectroscopy-based sensing of formaldehyde with porous TiO_2 under UV illumination, Sensors and Actuators B: Chemical, 185 (2013) 1-9.
27. J. Wang, Y. Shen, X. Li, Y. Xia, C. Yang, Synergistic effects of UV activation and surface oxygen vacancies on the room-temperature NO_2 gas sensing performance of ZnO nanowires, Sensors and Actuators B: Chemical, 298 (2019).
28. W. Li, J. Guo, L. Cai, W. Qi, Y. Sun, J.-L. Xu, M. Sun, H. Zhu, L. Xiang, D. Xie, T. Ren, UV light irradiation enhanced gas sensor selectivity of NO_2 and SO_2 using rGO functionalized with hollow SnO_2 nanofibers, Sensors and Actuators B: Chemical, 290 (2019) 443-452.
29. J.Saura, Gas-sensing properties of SnO_2 pyrolytic films subjected to ultraviolet radiation., Sensors and Actuarors B, 17 (1994) 211-214.
30. R. Kumar, X. Liu, J. Zhang, M. Kumar, Room-Temperature Gas Sensors Under Photoactivation: From Metal Oxides to 2D Materials, Nano-Micro Letters, 12 (2020).
31. Z. Li, J. Yi, Enhanced ethanol sensing of Ni-doped SnO_2 hollow spheres synthesized by a one-pot hydrothermal method, Sensors and Actuators B: Chemical, 243 (2017) 96-103.
32. S. Majumdar, P. Nag, P.S. Devi, Enhanced performance of CNT/SnO_2 thick film gas sensors towards hydrogen, Materials Chemistry and Physics, 147 (2014) 79-85.
33. K. Suematsu, M. Yuasa, T. Kida, N. Yamazoe, K. Shimanoe, Determination of Oxygen Adsorption Species on SnO_2: Exact Analysis of Gas Sensing Properties Using a Sample Gas Pretreatment System, Journal of The Electrochemical Society, 161 (2014) B123-B128.
34. A. Gurlo, Interplay between O_2 and SnO_2: oxygen ionosorption and spectroscopic evidence for adsorbed oxygen, Chemphyschem, 7 (2006) 2041-2052.
35. J.T. Chaonan Xu, Norio Miura and Noboru Yamazoe, Grain size effects on gas sensitivity of porous SnO_2-based elements, Sensors and Actuators B: Chemical, 3 (1991) 147-155.